

## A Simple Tri-Band MIMO Antenna Using a Single Ground Stub

Anjali A. Chaudhari<sup>1, \*</sup> and Rajiv K. Gupta<sup>2</sup>

**Abstract**—In this paper, a simple and compact tri-band multiple-input-multiple-output (MIMO) antenna for wireless applications is proposed. The antenna is composed of two symmetric monopoles placed a distance of  $0.106\lambda_0$  and occupies  $0.26\lambda_0 \times 0.25\lambda_0$  board area. The tri-arm monopole offers operation over 2.1–2.7 GHz, 3.3–3.7 GHz and 4.9–5.35 GHz with percentage impedance bandwidth of 25%, 11.4% and 8.7%, respectively. An isolation greater than 20 dB is achieved by integrating a stub in the ground plane and adding a stub in the feed line. The structure exhibits stable gain and radiation patterns. Various performance metrics including envelope correlation coefficient (ECC), diversity gain (DG) and mean effective gain (MEG) are measured.

### 1. INTRODUCTION

Continuous ascent in the sharing of intense content and real-time information through multimedia has promoted reliable and high data rate communication in the telecommunication field. In addition, many services introduced in the market demand wide bandwidth while the radio spectra is becoming a rare commodity. Multiple-input-multiple-output (MIMO), a radio communication technology, utilizes the available bandwidth more effectively [1]. More isolated, compact modern devices encompassing multiple applications lay down two major constraints in the design of MIMO structures. Supreme constraint is the limited antenna substantial size, resulting in the reduction of the inter-element spacing in the MIMO structures. But the close proximity of the elements lead to pronounced mutual coupling resulting in the performance degradation of the system [2]. Several systems with isolation enhancement techniques including defected ground structures, neutralization line, meta-materials, decoupling strips and extended ground plane have been researched over the years [3–9]. However, there is a trade-off in the size, bandwidth and design complexity in these mutual coupling reduction techniques. Another constraint is to design a multi-band antenna in order to support multifunctional operations for communication standards.

Several methods have been devised to design a solitary radiating structure to operate on a number of bands instead of supporting many applications dedicated antennas in a particular device. This leads to the evolution of antennas resonating at multiple frequencies [10–19]. A dual band dual polarized high isolation antenna offering more than 95% efficiency is proposed in [10]. Two element dual-band MIMO antenna with 20 dB isolation is stated in [11] where, each radiating element is F-shaped monopole while the isolation mechanisms consist of an elliptical slot and a parasitic patch. A microstrip line fed dual-band antenna using two unequal quarter wavelength slots featuring as radiators is proposed in [12]. In this antenna, a simple decoupling network consisting of a wide slit and a pair of narrow slots is employed to achieve isolation more than 20 dB. A 4-port dual-band MIMO slot antenna with 12 dB isolation operating at two WLAN frequencies is presented in [13]. A dual-band inverted-F MIMO antenna employs two meandering monopoles to obtain WLAN bandwidth while a meandering resonant

---

*Received 18 June 2018, Accepted 19 August 2018, Scheduled 27 August 2018*

\* Corresponding author: Anjali Ashish Chaudhari (anjalicbaudhari@sfitengg.org).

<sup>1</sup> Department of Electronics and Telecommunication Engineering, St. Francis Institute of Technology, Mumbai, India. <sup>2</sup> Department of Electronics and Telecommunication Engineering, Terna Engineering College, Navi-Mumbai, India.

arm and an inverted T-shaped branch on the ground plane form as decoupling devices to improve port isolation [14]. A system offering triple band characteristic is designed by loading a square loop antenna with CRLH unit cell [15] in which an isolation more than 15 dB is obtained by implementing an open ended I-shaped slot in the ground plane. A MIMO antenna incorporated with two symmetric triple-band antenna elements and two physical decoupling devices is reported in [16] wherein; each element is composed of three individual meander-line type inverted-L (MLIL) radiators corresponding to the specific triple frequency bands. On the other hand, mutual coupling due to spatial radiation and common ground plane is reduced by placing a winding meander line resonator in between the elements and a T-shaped slot cavity resonator in the ground plane. In [17], a PIFA coupled by L-shaped monopole is employed to achieve tri-band operation where the port isolation is enhanced by embedding slits in the ground plane. A tri-band MIMO antenna designed for WLAN/WiMAX applications uses symmetrically placed C-shaped monopoles as the radiating elements [18], and coupling reduction between the antenna elements is achieved by etching an ellipse ended step slot on the ground plane. A MIMO antenna composed of hexagonal patches or slots is designed to operate at multiple frequencies [19]. This arrangement contributed in reducing the mutual coupling more than 30 dB. However, the design of a compact multi-band MIMO antenna with significant isolation between the antenna elements is still a challenge for researchers.

In this paper, a simple and compact tri-band MIMO antenna with high isolation is proposed. The antenna provides tri-band response, and the operating bands can be independently controlled by altering the dimensions of the respective arms of the monopoles. A stub is integrated in the ground plane to realize isolation greater than 20 dB over 10 dB impedance bandwidths of 600 MHz (2.1–2.7 GHz), 400 MHz (3.3–3.7 GHz) and 450 MHz (4.9–5.35 GHz). In contrast to the systems considered in the literature, the proposed MIMO antenna is simple to design and occupies less board area.

## 2. DESIGN THEORY AND ANTENNA GEOMETRY

### 2.1. Design Theory

A multi-band monopole antenna can be designed using multiple branches in a monopole antenna. A tri-band antenna can be designed using three arms. An E-shaped tri-band antenna is reported in [20]. The longest arm of the antenna resonates at lowest frequency, while the shortest arm resonates at highest frequency. The resonant frequency depends on the length, while the bandwidth of a frequency band depends on the width of an arm. Thus, the three arms of an E-shaped antenna can independently control the three bands. Since the E-shaped antenna is symmetrical, one half of the E-shaped antenna can be removed, and half E-shaped antenna still offers the tri-band operation. Therefore, to have a compact MIMO antenna, a two-element half-E-shaped monopole antenna is designed as shown in Fig. 1.

Along with the compact size, high isolation between the antenna elements is an important requirement of MIMO antenna. Since the electrical distance between the two elements is least at lowest operating band, it is imperative to design a MIMO antenna to operate at lowest band (2.1–2.7 GHz) with high isolation. Therefore a single rectangular arm monopole antenna is designed to resonate at lowest desirable frequency. The length of the antenna is determined using Eq. (1) [21]. The resonant frequency depends on the length while the bandwidth depends on the width of the rectangular monopole. To accommodate the other element, the length of the ground plane is increased. To design a compact MIMO antenna, the second element is placed at about  $0.1\lambda_0$  apart from the first element, where  $\lambda_0$  is the wavelength in free space corresponding to the lowest operating frequency. The increase in length of the ground plane decreases the resonant frequency of antenna. The length of monopole is decreased to 70% of its original length so as to make the antenna to resonate at its initial frequency. The bandwidth of the antenna depends on the width of the rectangular arm.

To achieve at least 20 dB isolation between the two elements of antenna, a ground stub is integrated to the ground plane. This ground stub acts as reflector to the near fields and provides a decoupling path. The length of ground stub should be about 1.2 times the length of rectangular monopole so as to have the isolation more than 20 dB.

For antenna to operate over another band (3.3–3.7 GHz), a second arm is added to the first arm. Length of the arm is determined using Eq. (1) to resonate over middle band. However the length of the arm is decreased to counter the effect of increased ground plane length. Isolation  $> 20$  dB can be

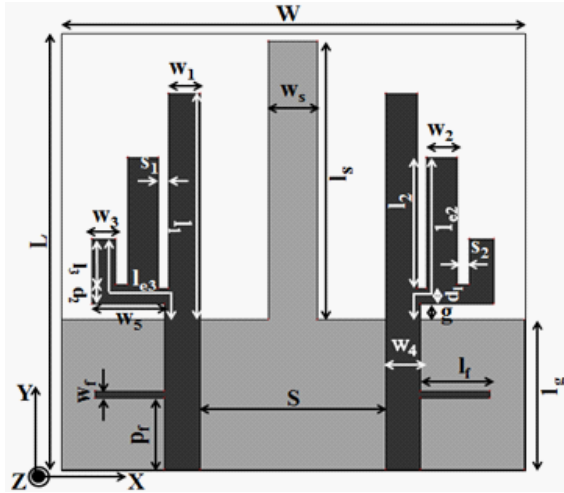


**Figure 1.** The proposed tri-band MIMO antenna.

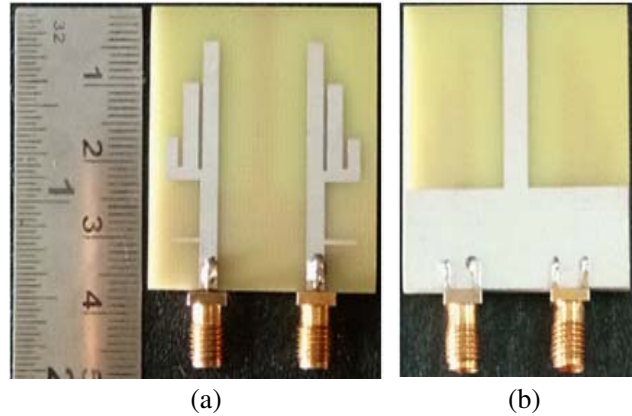


**Figure 2.** The fabricated MIMO antenna system: (a) top view and (b) bottom view.

achieved over middle band due to increase in the physical and electrical distance between the middle arms resonating at 3.5 GHz. Now, the third arm can be integrated to resonate at higher band (4.9–5.35 GHz). Antenna impedance matching, resonant frequency and bandwidth of three bands are tuned by integrating a  $\lambda/4$  open circuit stub in the feed line. This stub is designed to act as a band notch filter above the higher band. The stub length, width and position determine the resonant frequency and bandwidth of band notch filter [22, 23]. The resonant frequency of the band notch filter should be more than the resonant frequency of higher band and its bandwidth should be optimized to obtain the desired bandwidth of the higher band. The stub acts as a capacitor below its resonant frequency and therefore affects the resonant frequency of all the bands. The effect is more prominent in the higher band and little in the lower band. Based on this design theory, a tri-band MIMO antenna is designed which offers  $S_{11} < -10$  dB and  $S_{12} < -20$  dB over 2.1–2.7 GHz, 3.3–3.7 GHz and 4.9–5.35 GHz.

### 2.2. Antenna Geometry

The MIMO antenna is designed on an FR-4 substrate of 1.6 mm thickness with dielectric constant ( $\epsilon_r$ ) of 4.4 and loss tangent ( $\tan \delta$ ) of 0.02. The MIMO geometry is shown in Fig. 1 while the detailed antenna dimensions are listed in Table 1. The prototype of the proposed system is fabricated to verify the simulated results. The top and the bottom view of the fabricated MIMO antenna are shown in Fig. 2. The antenna occupies  $38 \times 37$  mm<sup>2</sup> board area and is realized using printed circuit board etching technique. The evolution stages of proposed antenna and the simulated  $S$ -parameters of each stage are shown in Fig. 3 and Fig. 4, respectively. ‘antenna 1’, a single band rectangular monopole with  $f_1$  as lowest frequency (corresponding to VSWR = 2) is designed. Its dimensions  $L = 29.4$  mm,  $W = 3$  mm,  $g = 0$  are determined using Eq. (1) [21].

$$f_l = \frac{7.2}{(L + (W/2\pi) + g) \times k} \text{GHz} \tag{1}$$

Here, the value of  $k = 1.15$  is considered for the FR-4 substrate. As illustrated in Fig. 4, the antenna offers a single band resonance at 2.1 GHz with higher order mode at 5.6 GHz. However, the radiation pattern at 5.6 GHz depicts higher order mode operation and consequently needs suppression. To accommodate the second element, ground plane dimensions are increased which results in ‘antenna 2’. In monopole antenna, the ground plane dimensions affect the resonating frequency and impedance bandwidth, therefore, the lower band shifts to 1.6 GHz due to increase in the ground plane dimensions. The length of the monopoles of ‘antenna 2’ is decreased by about 70% or 19.5 mm to increase the lowest operating frequency and to suppress the higher order mode. This results in ‘antenna 3’; however, the inter-element spacing of  $0.106\lambda_0$  leads to significant mutual coupling. In order to improve the isolation,

a rectangular stub is protruded from the ground plane thereby forming ‘antenna 4’. The length of the ground stub should be greater than the monopole length so that it acts as a reflector and reduce the mutual coupling due to near fields. This stub also provides a decoupling path and consequently limited amount of current couples to the neighbouring element due to surface waves. Fig. 5(a) portrays the surface current distribution in ‘antenna 4’ at 2.4 GHz for different lengths ( $l_s = 0.8l_1$  or  $l_1$  or  $1.2l_1$ ) of the ground stub, when one port of the antenna is excited while the other port is matched terminated with a load of  $50\ \Omega$ . The surface current and the near fields which get coupled to second element, decrease with increase in the length of ground stub. The ground stub length, about 20% more than the length of the monopole, results in mutual coupling  $< -20$  dB over the lower band from 2.1 GHz to 2.7 GHz. ‘antenna 5’ is evolved by integrating two arms to the already existing monopole in ‘antenna 4’. The effective length of two arms  $l_{e2}$  and  $l_{e3}$  corresponding to two bands are calculated using (1). The effective lengths are reduced and optimized due to the increased ground plane dimensions. This antenna operates over 3.33–4.02 GHz and 5.32–5.89 GHz bands in addition to the 2.15–2.9 GHz band.  $S_{11} < -10$  dB and  $S_{12} < -14$  dB is obtained over 5.32–5.89 GHz in ‘antenna 5’. Therefore, an improvement in the isolation and the impedance matching is required for the higher band. A stub in the feed line is introduced to improve the isolation in the higher band which results in the geometry of ‘antenna 6’. The feed line stub is designed to act as a  $\lambda/4$  open circuit stub at 6.5 GHz consequently behaving as a short circuit. Accordingly, return loss  $< 10$  dB and isolation greater than 24 dB are achieved over 4.9–5.35 GHz. In addition, the antenna also provides isolation more than 20 dB over the lower and middle bands.

**Table 1.** Dimensions of the proposed antenna.

<b>Parameter</b>	$L$	$W$	$S$	$l_1$	$l_2$	$l_3$	$w_1$	$w_2$	$w_3$	$l_{e2}$	$l_{e3}$
<b>Value (mm)</b>	37	38	15.2	19.5	11.3	3.9	2.6	2.5	2	14.8	9.2
<b>Parameter</b>	$d_1$	$d_2$	$G$	$w_4$	$w_5$	$w_s$	$l_s$	$l_f$	$p_f$	$w_f$	$l_g$
<b>Value (mm)</b>	1.4	1.7	1.3	3	6	4	24	5.7	6.2	0.6	13

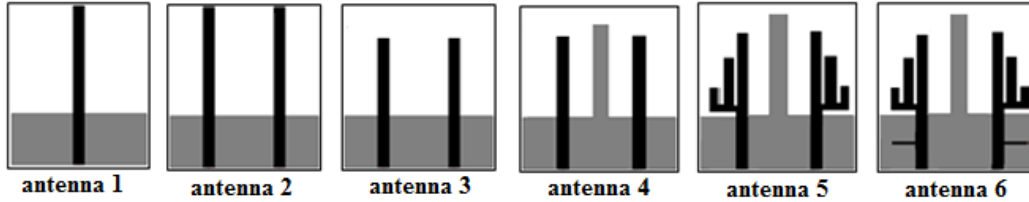


**Figure 3.** Evolution stages of proposed tri-band MIMO antenna.

This stub affects the impedance of antenna. The  $\lambda/4$  open circuit stub behaves as a capacitor below its resonance frequency of 6.5 GHz so the impedance is more capacitive than one without a stub. As a result, the resonant frequency of each of the three band decreases when stub is integrated in the feed line of ‘antenna 5’ as evident from Fig. 4. The stub acts as a band stop filter. The length, width and position of the stub affect the resonant frequency and bandwidth of band-stop filter, which in turn affects the impedance bandwidth of three bands. The effect of length, width and position of feed line stub is analyzed.  $S_{11}$  and  $S_{12}$  behavior against the parameter variations are displayed in Fig. 6. The stub length, width and position is optimized to 5.7 mm, 0.6 mm and 6.2 mm respectively so that the stub resonates at 6.5 GHz and electromagnetically couple with higher band to provide return loss  $< 10$  dB and isolation greater than 24 dB is achieved over 4.9–5.35 GHz.

The  $\lambda/4$  open circuit stub acts as a capacitor below 6.5 GHz, and as a result the resonance frequency of the three band decreases when the stub is introduced in ‘antenna 5’. As the length of the stub is decreased, the resonance frequency of the three bands increases. The effect is more prominent in the higher band than the lower band because at higher frequencies the decrease in stub length in terms of wavelength is more than lower frequencies, as evident from  $S_{11}$  plot of Fig. 6(a). Resonant frequency of

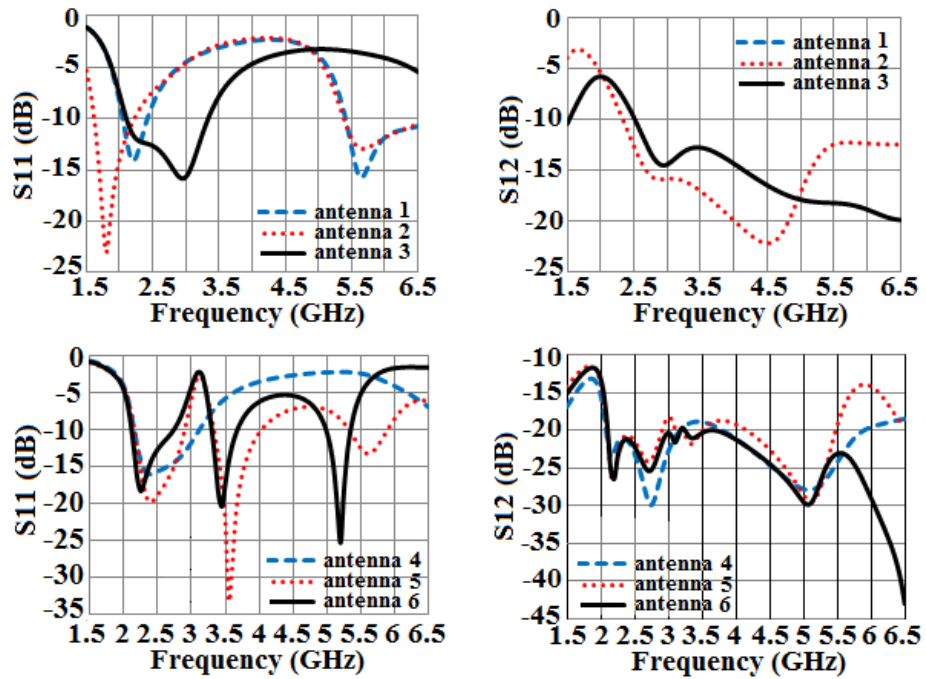


Figure 4.  $S_{11}$  and  $S_{12}$  of different antennas formed in the evolution of tri-band MIMO antenna.

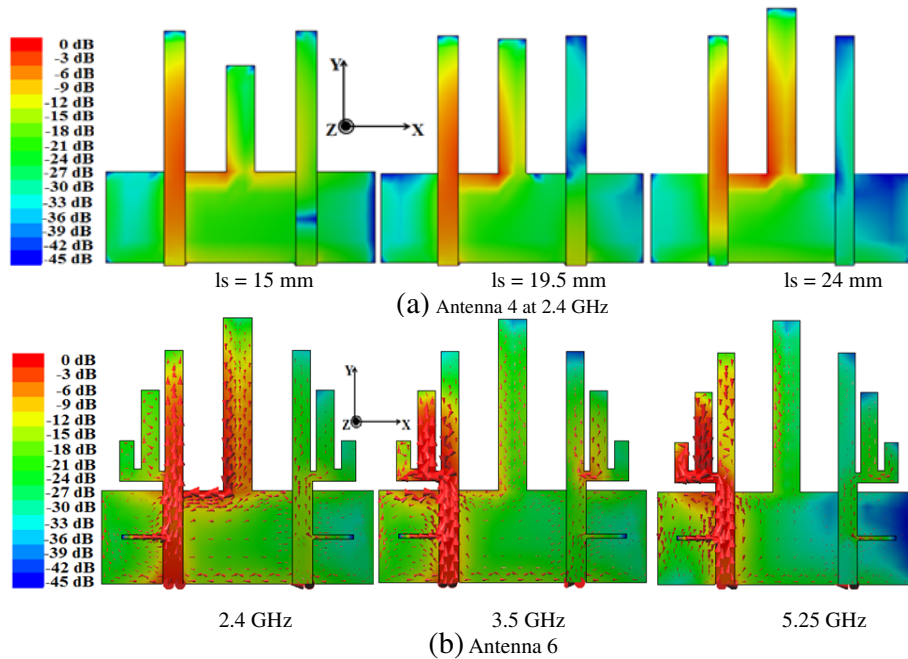
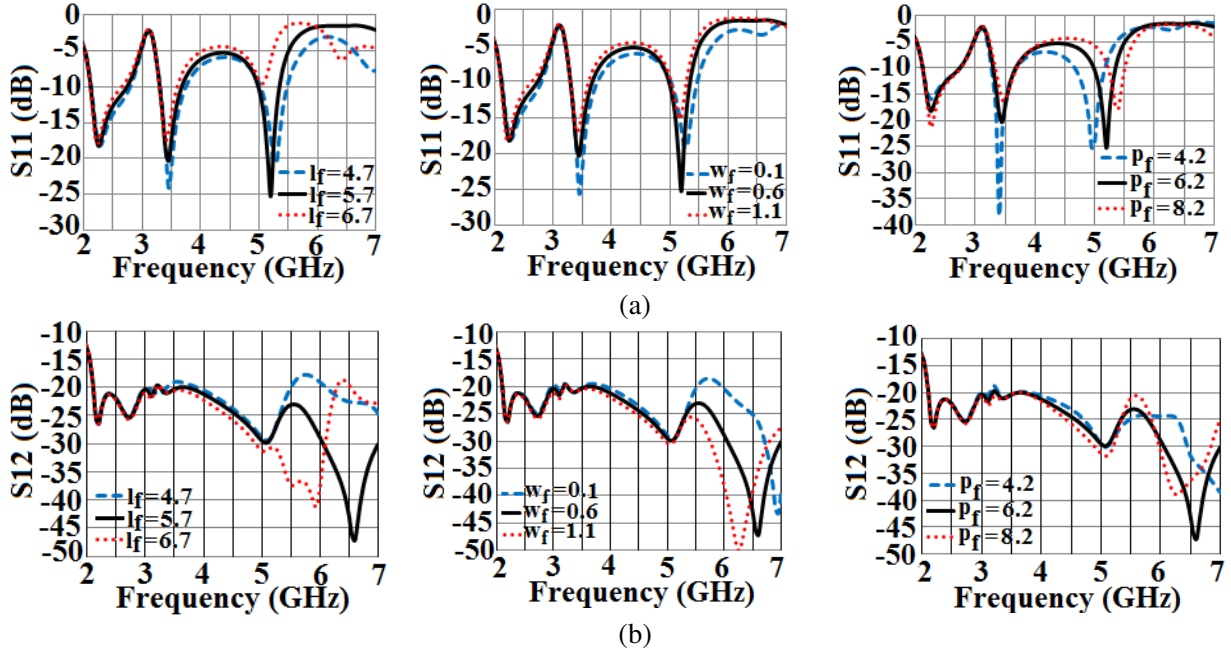


Figure 5. (a) Surface current distribution for different ground stub length and (b) vector surface current distribution for different frequencies.

the  $\lambda/4$  open circuit stub acting as a band stop filter decreases with increase in stub length as evident from  $S_{12}$  plot of Fig. 6(b).

The width of  $\lambda/4$  open circuit stub affects the resistive part of impedance. As the width of stub is decreased, the impedance becomes more resistive, and the impedance plot shifts to the right. As a result, the antenna resonates at higher frequency. Therefore, as the width of the stub is decreased the



**Figure 6.**  $S$ -parameters for different stub length  $l_f$ , stub width  $w_f$  and stub position  $p_f$  (a)  $S_{11}$  and (b)  $S_{12}$  (All dimensions are in mm).

resonance frequency of the three bands increases. The effect is more prominent in higher band than lower band as evident from the  $S_{11}$  plot of Fig. 6(a). The width of the  $\lambda/4$  open circuit stub affects the resonant frequency and bandwidth of the band stop filter. The resonant frequency decreases and bandwidth of band-stop filter increases with increase in stub width as evident from  $S_{12}$  plot of Fig. 6(b).

The  $\lambda/4$  open circuit stub position also affects the impedance of the antenna. When the stub is integrated, it introduces a capacitance which is formed between the radiating arms of antenna and the stub. When the stub is placed closer to the radiator, or as ' $p_f$ ' is increased, the capacitive effect increases, which results in the decrease in the resonant frequencies of three bands. The effect is more prominent in higher band than lower band as evident from  $S_{11}$  plot of Fig. 6(a). The stub position also affects the resonant frequency of the stub. The resonant frequency decreases when the stub is placed close to the radiating arm of the antenna due to increase in capacitive effect as evident from  $S_{12}$  plot of Fig. 6(b).

There is little change in  $S_{12}$  for stub position, length and width over the range of parameter variation as shown in Fig. 6(b), as antenna becomes non-responsive after 5.35 GHz due to feed stub. However, when the stub length is 6.7 mm, the stub resonates at 6 GHz, and its band notch bandwidth affects the higher band. It is observed that  $S_{12}$  actually improves in 4.9–5.35 GHz band, but  $S_{11}$  degrades.  $S_{11} > -10$  dB is obtained over 4.9–5.35 GHz. Therefore, the length, width and position of the feed stub affect the resonant frequency and the bandwidth of the band-stop filter which in turn affect the resonant frequency, impedance bandwidth and isolation of three bands. Without a stub,  $S_{11} < -10$  dB is obtained over 2.15–2.9 GHz, 3.3–4.0 GHz and 5.32–5.89 GHz bands, while  $S_{12} < -20$  dB,  $-18$  dB and  $-14$  dB are obtained over these bands respectively in 'antenna 5'. When stub is integrated in the feed line and its length, width and position are optimized,  $S_{11} < -10$  dB and  $S_{12} < -22$  dB,  $-20$  dB and  $-24$  dB are achieved over 2.1–2.7 GHz, 3.3–3.7 GHz and 4.9–5.35 GHz frequency bands, respectively.

The decrease in mutual coupling between the two elements in 'antenna 6' can be explained with the help of surface current distribution. The vector surface current distribution of 'antenna 6' at 2.4 GHz, 3.5 GHz and 5.25 GHz is depicted in Fig. 5(b). The longest arm of the tri-band antenna resonates at 2.4 GHz. The length and width of this arm affects the resonance frequency and the bandwidth of lower band [20]. The ground stub provides a decoupling path for the surface current due to surface waves and near fields. It also acts as a reflector to the near fields. As a result there is considerable current in the

ground stub which is  $180^\circ$  out of phase to the current in the radiating vertical arms of the monopole. The middle and smallest arm act as directors and the surface current in these arms are in phase with the current in the longest arm. The surface current in the ground stub is significant at 2.4 GHz. As a result, only a small amount of current couples to the other element despite the electrical separation between the two monopoles is least at 2.4 GHz.  $S_{12} < -22$  dB is obtained over the lower band from 2.1–2.7 GHz. There is significant horizontal current on the upper edge of the ground plane between the longest arm and the ground stub which affects the radiation pattern. The radiation pattern is directive towards  $-X$  axis when port 1 is excited, and port 2 is match terminated. Because of the significant horizontal current, along with the vertical current in the longest arm, the shapes of the radiation patterns are identical in  $X$ - $Z$  and  $Y$ - $Z$  planes.

The middle arm of the tri-band antenna resonates at 3.5 GHz. The length and width of middle arm affect the resonance frequency and the bandwidth of middle band [20]. At 3.5 GHz, though the magnitude of the current in the ground stub decreases, there is little surface current which couples to the other element due to increase in the physical distance between the middle arms resonating at 3.5 GHz. Beside this, the electrical distance also increases with increase in frequency. As a result,  $S_{12} < -20$  dB is obtained in the middle band from 3.3 to 3.7 GHz. There is significant horizontal current in the horizontal arm connecting the longest and middle arms. The current on the upper edge of the ground plane below this horizontal arm is  $180^\circ$  out of phase to the current in the horizontal arm of the monopole. Because of the significant horizontal current, along with the vertical current in middle arm, the shapes of the radiation patterns are identical in  $X$ - $Z$  and  $Y$ - $Z$  planes. The longest arm acts as a reflector for the middle arm resonating at 3.5 GHz. As a result, the surface current in longest arm is  $180^\circ$  out of phase to the current in the middle arm. Consequently, the radiation pattern is directive towards  $-X$  axis when port 1 is excited, and port 2 is match terminated.

The smallest arm resonates at 5.25 GHz. The length and width of this arm affects the resonant frequency and the bandwidth of lower band [20]. The surface current which couples to the other element further decreases, due to increase in physical and electrical separation between the smallest arms of the tri-band antenna. At 5.25 GHz, the middle and longest arms act as reflectors. As a result, the surface current in the longest and middle arms are  $180^\circ$  out of phase to the current in the smallest arm. At 5.25 GHz also, there is significant horizontal current in the horizontal arm connecting the three arms of the monopole which results in identical shapes of radiation patterns in  $X$ - $Z$  and  $Y$ - $Z$  planes. It is evident that the mutual coupling in ‘antenna 6’ is significantly reduced owing to the decrement in the surface current or near-field coupling due to ground stub.

### 3. FABRICATION AND MEASURED RESULTS

#### 3.1. Simulated and Measured $S$ -Parameters

The fabricated prototype is fed using the SMA connectors. The  $S$ -parameters are measured with Agilent 9916A network analyzer. The  $|S_{12}|$  measurement is carried out by exciting one port and match terminating the other port.

Simulated and measured  $S$ -parameters of the MIMO are shown in Fig. 7. It is evident that the results are in close agreement with each other.  $|S_{11}| < -10$  dB and  $|S_{12}| < -20$  dB are obtained for the desired operating bands viz. 2.1–2.7 GHz, 3.3–3.7 GHz and 4.9–5.35 GHz.

#### 3.2. Radiation Characteristics and Diversity Performance

The measured radiation patterns for  $\varphi = 0^\circ$  ( $X$ - $Z$ ) and  $\varphi = 90^\circ$  ( $Y$ - $Z$ ) planes at 2.4 GHz, 3.5 GHz and 5.25 GHz are shown in Fig. 8. The radiation patterns are measured in the  $X$ - $Z$  and  $Y$ - $Z$  planes, with port 1 or port 2 excited and the other port matched. The radiation patterns are stable and are mirror images of each other deciphering antenna diversity. Radiation patterns in  $Y$ - $Z$  plane and  $X$ - $Z$  plane are identical because there is significant horizontal surface current either along the edge of the ground plane or in the horizontal arm connecting the vertical arms of the monopole, along with the current in vertical arm at 2.4 GHz, 3.5 GHz and 5.25 GHz, as evident from the vector surface current distribution shown in the Fig. 5(b). The simulated and measured gains of the proposed structure are shown in Fig. 9(a). The gain variation is less than 2 dB over the operating bands with more than 80%

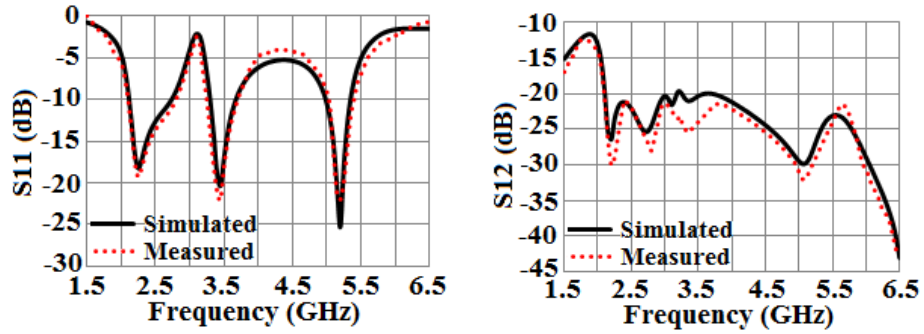


Figure 7. Simulated and measured  $S$ -parameters.

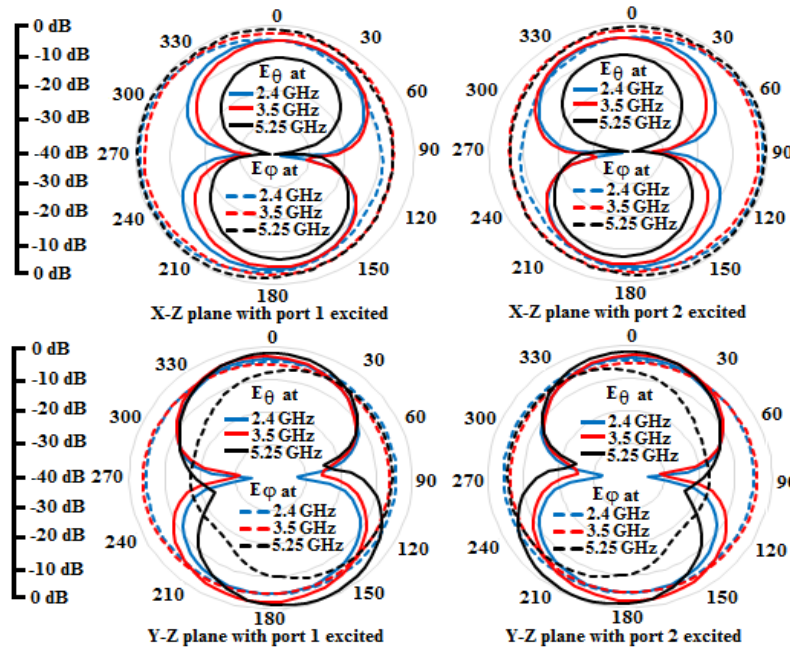


Figure 8. Measured radiation patterns.

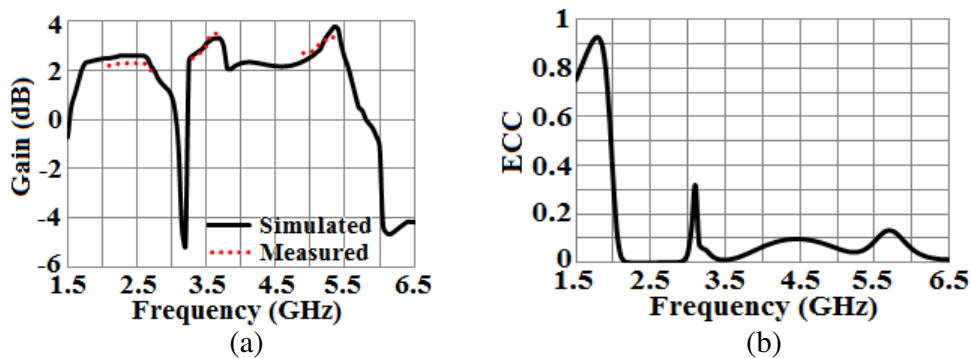


Figure 9. Simulated and measured results: (a) gain and (b) ECC of the proposed structure.

radiation efficiency. The diversity performance of the antenna system is analyzed by computing or measuring envelope correlation coefficient (ECC), diversity gain (DG) and mean effective gain (MEG).

An improvement in fading can be achieved when the signals received from the antenna satisfy the

following criteria [24].

$$ECC < 0.5 \tag{2}$$

$$MEG_i/MEG_j \cong 1 \tag{3}$$

ECC between the *i*th and *j*th elements is one of the figures of merit of a MIMO quantifying the correlation between the radiation patterns of the antenna elements. Thus, its evaluation takes into account the 3-dimensional radiation pattern rearranged in Equation (4).

$$ECC \approx A/(B \cdot C) \tag{4}$$

$$\begin{aligned} \text{Where } A &= \left[ \int_0^{2\pi} \int_0^\pi \left\{ \begin{aligned} &XPR \cdot E_{\theta i}(\theta, \varphi) E_{\theta j}^*(\theta, \varphi) P_\theta(\theta, \varphi) \\ &+ E_{\varphi i}(\theta, \varphi) E_{\varphi j}^*(\theta, \varphi) P_\varphi(\theta, \varphi) \end{aligned} \right\} \sin(\theta) d\theta d\varphi \right]^2 \\ B &= \left[ \int_0^{2\pi} \int_0^\pi \left\{ \begin{aligned} &XPR \cdot E_{\theta i}(\theta, \varphi) E_{\theta j}^*(\theta, \varphi) P_\theta(\theta, \varphi) \\ &+ E_{\varphi i}(\theta, \varphi) E_{\varphi j}^*(\theta, \varphi) P_\varphi(\theta, \varphi) \end{aligned} \right\} \sin(\theta) d\theta d\varphi \right]^2 \\ C &= \left[ \int_0^{2\pi} \int_0^\pi \left\{ \begin{aligned} &XPR \cdot E_{\theta i}(\theta, \varphi) E_{\theta j}^*(\theta, \varphi) P_\theta(\theta, \varphi) \\ &+ E_{\varphi i}(\theta, \varphi) E_{\varphi j}^*(\theta, \varphi) P_\varphi(\theta, \varphi) \end{aligned} \right\} \sin(\theta) d\theta d\varphi \right]^2 \end{aligned}$$

MEG of the *i*th and *j*th antenna elements can be expressed as Eq. (5),

$$MEG = \int_0^{2\pi} \int_0^\pi \left\{ \frac{XPR}{1 + XPR} G_\theta(\theta, \varphi) P_\theta(\theta, \varphi) + \frac{1}{1 + XPR} G_\varphi(\theta, \varphi) P(\theta, \varphi) \right\} \sin \theta d\theta d\varphi \tag{5}$$

DG can be evaluated using Eq. (6) [25],

$$DG = 10e_\rho \text{ with } e_\rho = \sqrt{1 - |ECC|} \tag{6}$$

**Table 2.** Computed MEGs for isotropic environment, ECC and DG at resonant frequencies.

<i>f</i> (GHz)	ECC	DG (dB)	MEG <sub>1</sub> (dB)	MEG <sub>2</sub> (dB)	MEG <sub>1</sub> /MEG <sub>2</sub>
2.4	0.00002	9.99	-3.3482	-3.3616	0.0134
3.5	0.0122	9.94	-3.6505	-3.6638	0.0133
5.25	0.0435	9.77	-3.9278	-3.9134	0.0144

**Table 3.** Comparison of the proposed MIMO antenna with reported multi-band designs.

Ref.	Approach	Antenna Size (mm <sup>2</sup> )	Bandwidth (GHz)	Electrical Size (λ <sub>o</sub> × λ <sub>o</sub> )	I <sub>min</sub> (dB)	ECC
[7]	Decoupling strips + Slotted ground	58 × 45	2-11/BN <sub>1</sub> = 3.3-3.6/BN <sub>2</sub> = 5-6/BN <sub>3</sub> = 7.2-8.4	0.38 × 0.3	15	0.01
[13]	Decoupling slits	20 × 46	2.4-2.5/4.9-5.75	0.16 × 0.37	12	0.27
[14]	Meander branch + T-shaped slot	52 × 77.5	2.4-2.48/5.15-5.825	0.42 × 0.62	15	0.2
[15]	Defected ground structure	45 × 25	2.37-2.64/3.39-3.58/4.86-6.98	0.36 × 0.2	15	0.012
[19]		64 × 35	<i>f</i> <sub>r1</sub> = 4.75/ <i>f</i> <sub>r2</sub> = 5.89/ <i>f</i> <sub>r3</sub> = 6.74/ <i>f</i> <sub>r4</sub> = 8.25/ <i>f</i> <sub>r5</sub> = 9.82	1.01 × 0.55	21.5	0.0004
[16]	Meander branch + T-slot	65 × 100	0.88-0.92/1.78-1.81/2.45-2.62	0.19×0.29	16	0.3
[17]	Ground slits	120 × 80	0.81-0.965/1.56-3.32/ 3.4-3.59	0.32 × 0.22	11	0.2
[18]		50 × 50	2.3-2.75/3.4-3.75/4.8-6	0.38 × 0.38	18	0.03
<b>P.W</b>	<b>Ground Stub</b>	<b>38 × 37</b>	<b>2.1-2.7/3.29-3.67/ 4.9-5.35</b>	0.26 × 0.25	<b>20</b>	<b>0.05</b>

where,  $e_\rho$  is an expression for the correlation efficiency, and CC is the correlation coefficient.

The ECC plot is shown in Fig. 9(b) while the diversity performance metrics at 2.4 GHz, 3.5 GHz and 5.25 GHz are listed in Table 2.  $ECC < 0.071$  over the three operating bands.

The proposed MIMO antenna is compared with the other reported antenna structures with respect to physical and the electrical size, bandwidth, isolation and ECC in Table 3. The proposed tri-band MIMO design is comparatively better in terms of size and exhibits a greater isolation than the structures proposed in [7, 13–19]. The design projected in [19] offers a better isolation but occupies a large board area. On the contrary, antennas in [13] and [15] engage less space at the cost of isolation. In addition, [13] and [14] present dual-band operation while the proposed antenna offers triple band performance with a relatively simple design.

#### 4. CONCLUSION

A simple to design symmetrically placed dual-element MIMO antenna for wireless applications is presented in this paper. The radiating monopole composed of three arms regulates the tri-band operation (2.1–2.7 GHz, 3.3–3.7 GHz and 4.9–5.35 GHz) arbitrated by  $|S_{11}| < -10$  dB. An isolation of 20 dB is attained using a single rectangular ground stub and a feed stub in the three bands of interest. The evaluated MEGs, diversity gain and correlation coefficient substantiate the MIMO performance of the antenna.

#### REFERENCES

1. Molisch, A. F. and M. Z. Win, "MIMO systems with antenna selection," *IEEE Micro. Mag.*, Vol. 5, No. 1, 46–56, March 2004.
2. Browne, D. W., M. Manteghi, M. P. Fitz, and Y. Rahmat-Samii, "Experiments with compact antenna arrays for MIMO radio communications," *IEEE Trans. Antennas Propag.*, Vol. 54, No. 11, 3239–3250, Nov. 2006.
3. Shoaib, S. S., I. Shoaib, X. Chen, and C. G. Parini, "Design and performance study of a dual-element multi-band printed monopole antenna array for MIMO terminals," *IEEE Antennas Wireless Propag. Lett.*, Vol. 13, 329–332, 2014.
4. Tripathi, S., A. Mohan, and S. K. Yadav, "A compact MIMO/Diversity antenna with WLAN band-notch characteristics for portable UWB applications," *Progress In Electromagnetics Research C*, Vol. 77, 29–38, 2017.
5. See, C. H., R. A. A-Alhameed, Z. Z. Abidin, N. J. McEwan, and P. S. Excell, "Wideband printed MIMO/diversity monopole antenna for WiFi/WiMAX Applications," *IEEE Trans. Antennas Propag.*, Vol. 60, No. 4, 2028–2035, April 2012.
6. Sharawi, M. S., A. B. Numan, and D. N. Aloï, "Isolation improvement in a dual-band dual-element MIMO antenna system using capacitively loaded loops," *Progress In Electromagnetics Research*, Vol. 134, 247–266, 2013.
7. Jaglan, N., S. D. Gupta, B. K. Kanaujia, S. Srivastava, and E. Thakur, "Triple band notched DG-CEBG structure based UWB MIMO/diversity antenna," *Progress In Electromagnetics Research C*, Vol. 80, 21–37, 2018.
8. Shoaib, S., I. Shoaib, N. Shoaib, X. Chen, and C. G. Parini, "MIMO antennas for mobile handsets," *IEEE Antennas Wireless Propag. Lett.*, Vol. 14, 799–802, 2015.
9. Jetti, C. R. and V. R. Nandanavanam, "A very compact MIMO antenna with triple band-notch function for portable UWB systems," *Progress In Electromagnetics Research C*, Vol. 82, 13–27, 2018.
10. Kashani, F. H., M. Shahpari, and H. Ameri, "Dual band dual polarized antenna with high efficiency for base transceiver stations," *Journal of Electromagnetic Waves and Appl.*, Vol. 23, No. 10, 1371–1379, 2008.

11. Nirmal, P. C., A. B. Nandgaonkar, S. Nalbalwar, and R. K. Gupta, "A compact dual band MIMO antenna with improved isolation for Wi-Max and WLAN applications," *Progress In Electromagnetics Research M*, Vol. 68, 69–77, 2018.
12. Nandi, S. and A. Mohan, "A compact dual-band MIMO slot antenna for WLAN applications," *IEEE Antennas Wireless Propag. Lett.*, Vol. 16, 2457–2460, 2017.
13. Soltani, S., P. Lotfi, and R. D. Murch, "A dual-band multi-port MIMO slot antenna for WLAN applications," *IEEE Antennas Wireless Propag. Lett.*, Vol. 16, 529–532, 2017.
14. Deng, J. Y., J. Y. Li, L. Zhao, and L. X. Guo, "A dual-band inverted-F MIMO antenna with enhanced isolation for WLAN," *IEEE Antennas Wireless Propag. Lett.*, Vol. 16, 2270–2273, 2017.
15. Nandi, S. and A. Mohan, "CRLH unit cell loaded tri-band compact MIMO antenna for WLAN/WiMAX applications," *IEEE Antennas Wireless Propag. Lett.*, Vol. 16, 1816–1819, 2017.
16. Sun, J. S., H. S. Fang, P. Y. Lin, and C. S. Chuang, "Triple-band MIMO antenna for mobile wireless applications," *IEEE Antennas Wireless Propag. Lett.*, Vol. 15, 500–503, 2016.
17. Zhu, J., B. Feng, L. Deng, B. Peng, and S. Li, "Coupled-fed tri-band MIMO mobile antenna for WWAN and LTE applications," *Microwave and Optical Technology Lett.*, Vol. 59, No. 2, 463–468, 2017.
18. Fang, Q., D. Mi, and Y.-Z. Yin, "A tri-band MIMO antenna for WLAN/WiMAX application," *Progress In Electromagnetics Research Letters*, Vol. 55, 75–80, 2015.
19. Srinivasa Rao, S., K. J. Babu, and A. M. Prasad, "Compact multi-band MIMO antenna with improved isolation," *Progress In Electromagnetics Research M*, Vol. 62, 199–210, 2017.
20. Gupta, R. K., "Printed tri-band monopole antenna structures for wireless applications," *Microwave and Optical Technology Lett.*, Vol. 51, No. 7, 1781–1785, 2009.
21. Ray, K. P., "Design aspects of printed monopole antennas for ultra-wide band applications," *International Journal of Antennas and Propagation*, Vol. 2008, 1–8, March 2008.
22. Mishra, S. K., R. K. Gupta, A. R. Vaidya, and J. Mukherjee, "Parallel metal plated U-shape ultra-wide band antenna with WLAN band-notched characteristics," *PIERS Proceedings*, 1846–1851, Kuala Lumpur, Malaysia, March 27–30, 2012.
23. Mishra, S. K. and J. Mukherjee, "Compact printed dual band-notched U-shaped UWB antenna," *Progress In Electromagnetics Research C*, Vol. 27, 169–181, 2012.
24. Ghosh, S., T. N. Tran, and T. L. Ngoc, "Minaturized four-element diversity PIFA," *IEEE Antennas Wireless Propag. Lett.*, Vol. 12, 396–400, March 2013.
25. Kharche, S. U., G. S. Reddy, B. Mukherjee, R. K. Gupta, and J. Mukherjee, "MIMO antenna for Bluetooth, Wi-Fi, Wi-Max and UWB applications," *Progress In Electromagnetics Research C*, Vol. 52, 53–62, 2014.